PERGAMON

Journal of Structural Geology 24 (2002) 1029–1043

JOURNAL OF STRUCTURAL GEOLOGY

www.elsevier.com/locate/jstrugeo

Experimental study of syntaxial vein growth during lateral fluid flow in transmitted light: first results

Christoph Hilgers*, Janos L. Urai

Geologie-Endogene Dynamik, RWTH Aachen, D-52056, Germany

Received 6 November 2000; revised 23 April 2001; accepted 27 April 2001

Abstract

In-situ observations of transmitted-light experiments of syntaxial vein growth during lateral fluid flow in a simulated fracture show a decrease in growth rate towards the downstream end. As a consequence, the fracture is sealed at the inlet. Our observations show the rapid, non-linear growth competition of grains, which is a result of anisotropic growth kinetics and the complex fluid flow around the individual crystals.

We compared our results with simulations based on a simplified numerical model, which builds on existing simulation techniques of this system. The model incorporates plug flow and a fluid-flow velocity dependent crystal growth rate law based on literature data. Simulations are in reasonable agreement with experimental results. A sensitivity analysis shows that a high fluid flow velocity and a low supersaturation increase the potential to seal a vein homogeneously, in agreement with previous work. Additionally, the effect of the initial crack shape is explored.

Keywords: Syntaxial vein growth; Lateral fluid flow; Sealing experiments

1. Introduction

Veins are common structures in the Earth's crust, formed by crystal growth from supersaturated fluids in dilation sites. They play a key role in the accumulation of both ore and hydrocarbon deposits and are therefore of economic interest. Geologists use veins for analyses of crustal fluid systems and deformation processes (Ramsay and Huber, 1983; Cox, 1999). However, understanding of the processes during vein formation is limited. This is due to the complex interplay of different processes related to:

- Transport (advection vs. diffusion; permeability evolution under changing fluid pressure; Wiltschko et al., 1998).
- Crystal growth dynamics (supersaturation vs. precipitation rate; maintenance of supersaturation by parameters such as additives, fluid salinity, complexing, clay coating, pore size, partial pressure of CO_2, redox or pH conditions; Ellis and Mahon, 1977; Nicholson, 1993; Whitworth and Fritz, 1994; Ortoleva et al., 1995; Putnis et al., 1995; Gutjahr et al., 1996; Deleuze and Brantley, 1997; Kharaka et al., 1999; Whitworth et al., 1999; Herrmann, 2000; Hilgers, 2000; Wiltschko and Morse, 2001).
- Microstructural evolution (growth competition and the development of crystallographic preferred orientation; the effects of complex boundary conditions for crystal growth such as dilation vs. growth rate, the formation of fibrous veins and possible feedback by the force of crystallisation; the effects of dislocation densities of the seed crystals; Mügge, 1928; Schmidegg, 1928; Urai et al., 1991; Thijssen et al., 1992; Ristic et al., 1997; Bons, 2000; Koehn et al., 2000; Hilgers et al., 2001).

Such a complex system can be expected to evolve in many different directions, and the literature accordingly contains a large number of vein formation scenarios.

1.1. Advective transport models

In seismic pumping (Sibson et al., 1975) the fluid migrates down a potential gradient into a dilation site, opened by accumulating differential stress or increasing fluid pressure. While quartz precipitates in the dilation site mainly due to the decrease in fluid pressure, other minerals like calcite show more complex behaviour. A collapse of the dilation site expels the fluid upwards through a fault or adjacent fractures, also leading to mineral precipitation as

* Corresponding author. Fax: +49-241-8092-358.
E-mail address: c.hilgers@ged.rwth-aachen.de (C. Hilgers).

0191-8141/02/$ - see front matter
PII: S0191-8141(01)00089-X

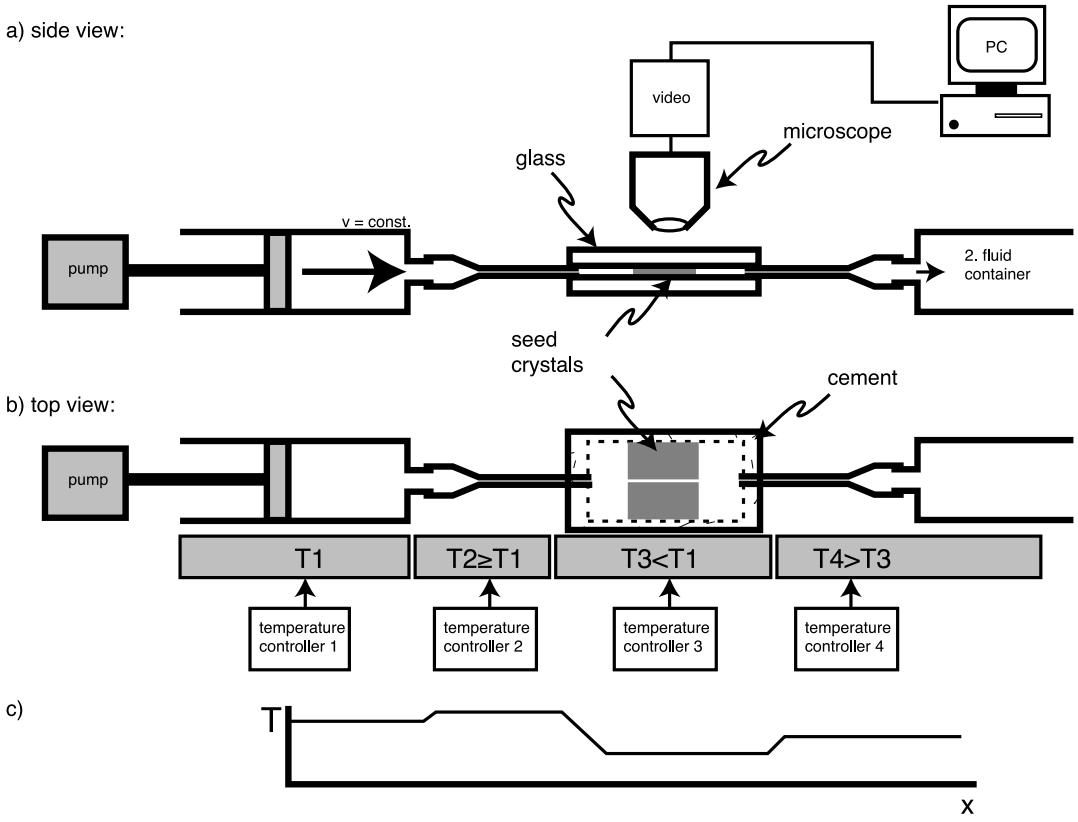

Fig. 1. Sketch of the experimental set-up. Fluid is pumped through a tube into a small, transparent reaction cell (a, b). Due to a temperature decrease (c) material precipitates in the reaction cell on the seed crystals. The seed crystals are made of two porous blocks of alum crystals, separated by a small channel. Lateral fluid flow and supersaturation due to a temperature decrease results in syntaxial growth in this channel.

a result of decreasing fluid pressure. This collapse is driven by a gradient in fluid pressure in the wall rock being transiently less than fluid pressure in the dilation site, and partly by stress distributions around the dilation site which cause spalling.

The active role of the dilation site is described by the suction pumping model (Sibson, 1990a), where opening rates of the dilation site are faster than the fluid can flow. Thus a temporary underpressure in the void develops, working against the opening of the void and driving fluid into the dilation site. Quartz precipitates due to decreasing fluid pressure.

Etheridge et al. (1984) presented a matrix-to-crack pumping model, where vein opening takes place in regions with local fluid pressure significantly over hydrostatic (overpressure cells; Bradley and Powley, 1994; Ortoleva, 1994; Burrus, 1998). The resulting local potential gradient also drives precipitation of material in the vein.

The fault-valve mechanism of Sibson (1990b, 1995) needs a low permeable barrier, which caps a zone with near-lithostatic fluid pressure in the footwall. Fluid pressure build-up results in extensional failure and fluid discharge once the minimum effective stress exceeds the tensile strength of the low permeable barrier. During this channelled flow the fluid may re-seal the path across the low permeable barrier and produce a cyclically self-sealing system. Yardley (1983) proposed a similar model on a smaller scale, with cyclic hydraulic fracturing due to self-sealing and rapid flow of non-equilibrated fluid along a pressure gradient.

Lee et al. (1996) and Lee and Morse (1999) experimentally investigated crystallisation from a supersaturated solution of calcite flowing along a channel bounded by calcite grains, in an attempt to model a single step of the cyclic models outlined above. Based on measurements of the fluid properties (concentration, pH, alkalinity) at the inlet and the outlet in combination with photomicrographs of the crystals, the authors give a quantitative discussion of the process, which agrees well with their measurements. Using this model, the authors then make predictions of the sealing of natural fractures. They conclude that uniform precipitation along the vein wall can be obtained either by low supersaturation or high fluid flow velocity, but note that such a low degree of supersaturation requires unreasonably high fluid volumes to fill natural veins in geologic time.

In the last five years significant advances have been achieved in numerical modelling of precipitation and dissolution of reactive solutes in fractures. A review of recent developments is given by Lasaga (1998) and Dijk and

Berkowitz (1998). They present a range of simulations where the relative importance of advection, diffusion and reaction kinetics is varied. The importance of these processes can be characterised by the local values of two dimensionless numbers. The Peclet number, defined as $Pe = v_{flow}y/D_m$ where v_{flow} is the fluid flow velocity, y is the fracture aperture and D_m the molecular diffusion coefficient, describes the relative importance of advection and diffusion on solute transport. Above the critical value of $Pe \approx 10$ advection becomes dominant. The Damköhler number, defined as $Da = ky^2/D_m$, where k is the first order kinetic reaction rate coefficient, describes the relative importance of diffusion and reaction kinetics. Above the critical value of $Da \approx 3$ reaction kinetics become dominant.

1.2. Diffusive transport models

The second end-member transport mechanism during vein growth is by diffusion in a static fluid. As is the case for the advective transport models, several scenarios have been presented.

It has long been known that fibrous crystals form when solvent evaporates from a porous substrate filled with saturated solution. For example, Kenngott (1855) wrote: "*I noticed that the lime painting peeled off and that it was lifted… Bricks and roughcast are more porous than the lime painting, and this [painting] forms a coherent layer… The little amount of water, which penetrated the bricks became rigid, crystallised, and forced an opening of the gap between roughcast and painting… The ice… was in its mass parallel fibrous, similar to veins composed of salt, gypsum or calcite… The linear crystals received their continuous growth at their base.*" (translation by the authors). Another early example is Schmidt (1911): "*Correctly here he [a publication by Kuhlmann from 1860] points to the importance of capillarity, slow evaporation and the porosity of the clay for the formation of such [halite] fibres*" (translation by the authors). Taber (1916) presented a series of experiments on fibrous growth. This system seems to require a two-phase pore-fill (liquid and air) with capillary forces having an important controlling role.

At depths where unsaturated pore fill is not possible, crystal growth from a stationary supersaturated solution was proposed by Durney and Ramsay (1973). This process is envisaged to be related to solution transfer creep processes (Gratier et al., 1994; Hickman and Evans, 1995), where material dissolved in sites of high normal stress diffuses through the pore fluid and precipitates in the dilation site.

Fisher and Brantley (1992) extended the cyclic flow model by incorporating matrix-to-crack diffusion on a small scale, this concentration gradient being driven by the pressure gradient between vein fluid and pore fluid.

Crystals grown from a supersaturated solution are able to lift a weight, and this force of crystallisation is believed in some situations to cause vein opening. As far as we know, the first account of this is given by Bunsen (1847): "*Alone the low solubility of this salt [gypsum], combined with the large ability of crystallisation, causes its continuous precipitation, and this under odd conditions… This gypsum is exposed in continuous layers… and is in its appearance completely identical with gypsum layers often found in marl and clay of the Triassic formation… The formation of crystals thus enters the field of mechanical forces, because forming gypsum intercalations lift the fluid-saturated clay*" (translation by the authors); further work in this field was presented by Taber (1918), Correns and Steinborn (1939), Correns (1949) and Means and Li (2001).

It is thus clear that epitaxial growth of crystals on the wall of a fracture during lateral flow of a supersaturated fluid is one of the important processes during vein accumulation. At present our understanding of this system is limited, especially in the field of microstructural evolution. Our study attempts to contribute here.

In this paper we present the first results of an experimental study of syntaxial vein growth in an apparatus that allows real time in-situ observation of the growing crystals in transmitted light microscopy. Quantitative analysis of the syntaxial vein growth of a cubic model material ($KAl(SO_4)_2 \times 12H_2O$) during lateral fluid flow shows the details of the growth competition process, superimposed on the previously documented decrease of growth rate along the fracture due to depletion of the fluid.

We further present a simple model of crystal growth from a fluid flowing along a fracture, together with finite difference numerical solutions of this model for the conditions of our experiment. In this numerical model, which is a variation of the general solution presented by Lasaga (1998) and Dijk and Berkowitz (1998) (see also Lee et al., 1996), we quantify the effects of the parameters fluid flow velocity, supersaturation and growth rate on the resulting microstructure. Finally we discuss the implications of our results to vein sealing in nature.

2. Experimental techniques

The apparatus consists of a micro-pump containing a few millilitres of saturated solution and crystals of alum ($KAl(SO_4)_2 \times 12H_2O$, Carl Roth GmbH & Co., $\geqq 97.5\%$ quality). Saturation was ensured by stirring the solution and crystals for 2 days, before filling the micro-pump. The pump is driven by a synchronous motor at constant speed (1/3 RPH), producing controlled rate fluid flow via a small tube into a thin, transparent reaction cell. The discharge is collected in a second fluid container. Typical parameters in our experiments are 0.2 mm/s initial fluid velocity in the cell at a fluid flux of about 0.032 mm^3/s.

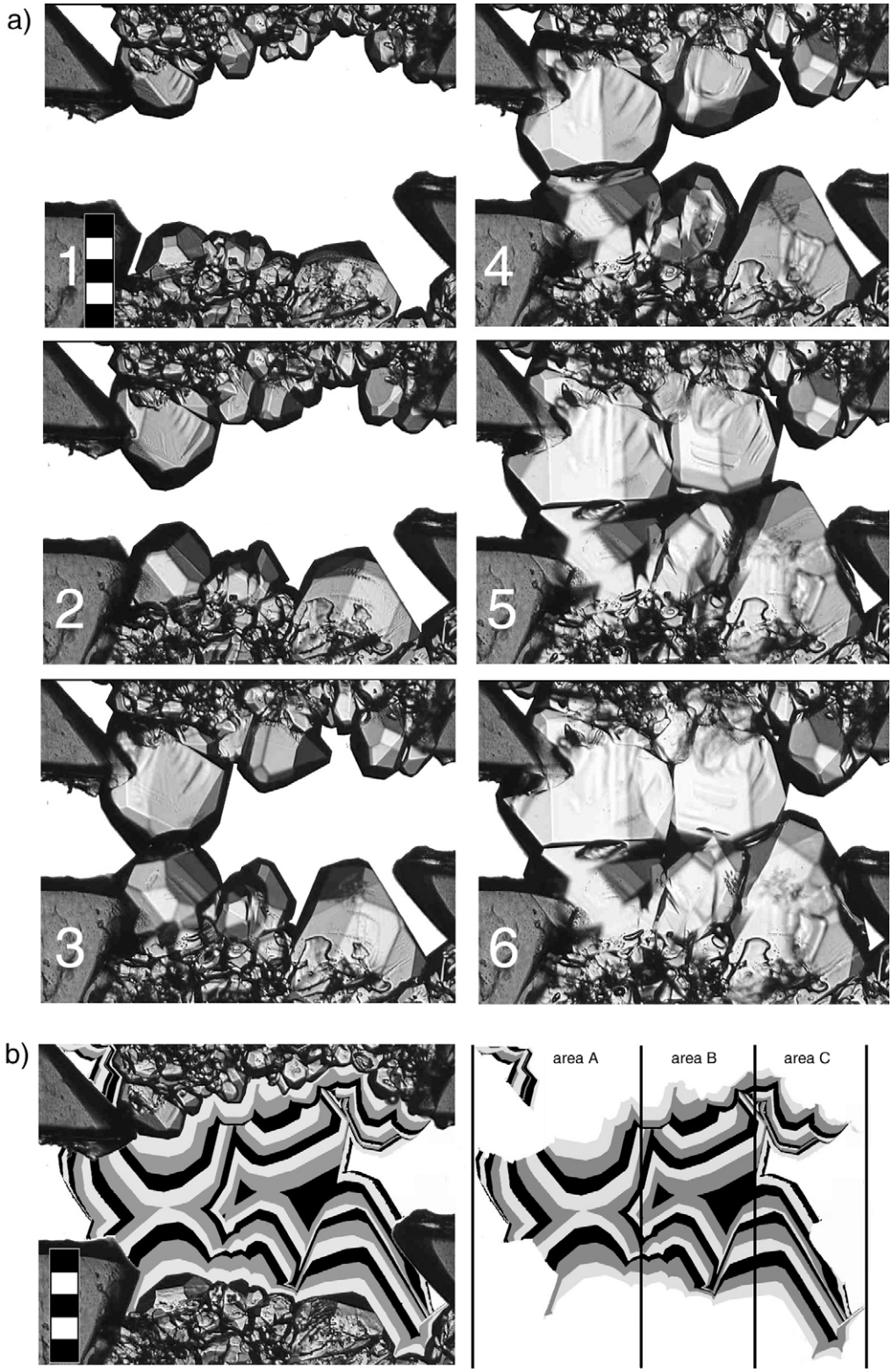

Fig. 2. (a) Microstructural evolution of the experimental run, with a 1 h time gap between the images until complete vein closure after 5.5 h. Seed crystals at the top and the bottom continue outside the field of view. Fluid flows from left to right. After 2.5 h, two facing crystals at the inlet touch each other, but fluid flow and growth continues until the vein is completely sealed (after 5.5 h). Then, the crystals have sealed all pores and the vein–glass interface, and further flow is blocked. Scale bar: 0.5 mm. (b) Time series of the same experiment, with each grey tone representing the grown area after 30 min. The grown material was calculated in three sub-areas (A: inlet, B; centre, and C: outlet) for a calculation of the growth rate (see Figs. 3 and 4). Scale bar: 0.5 mm.

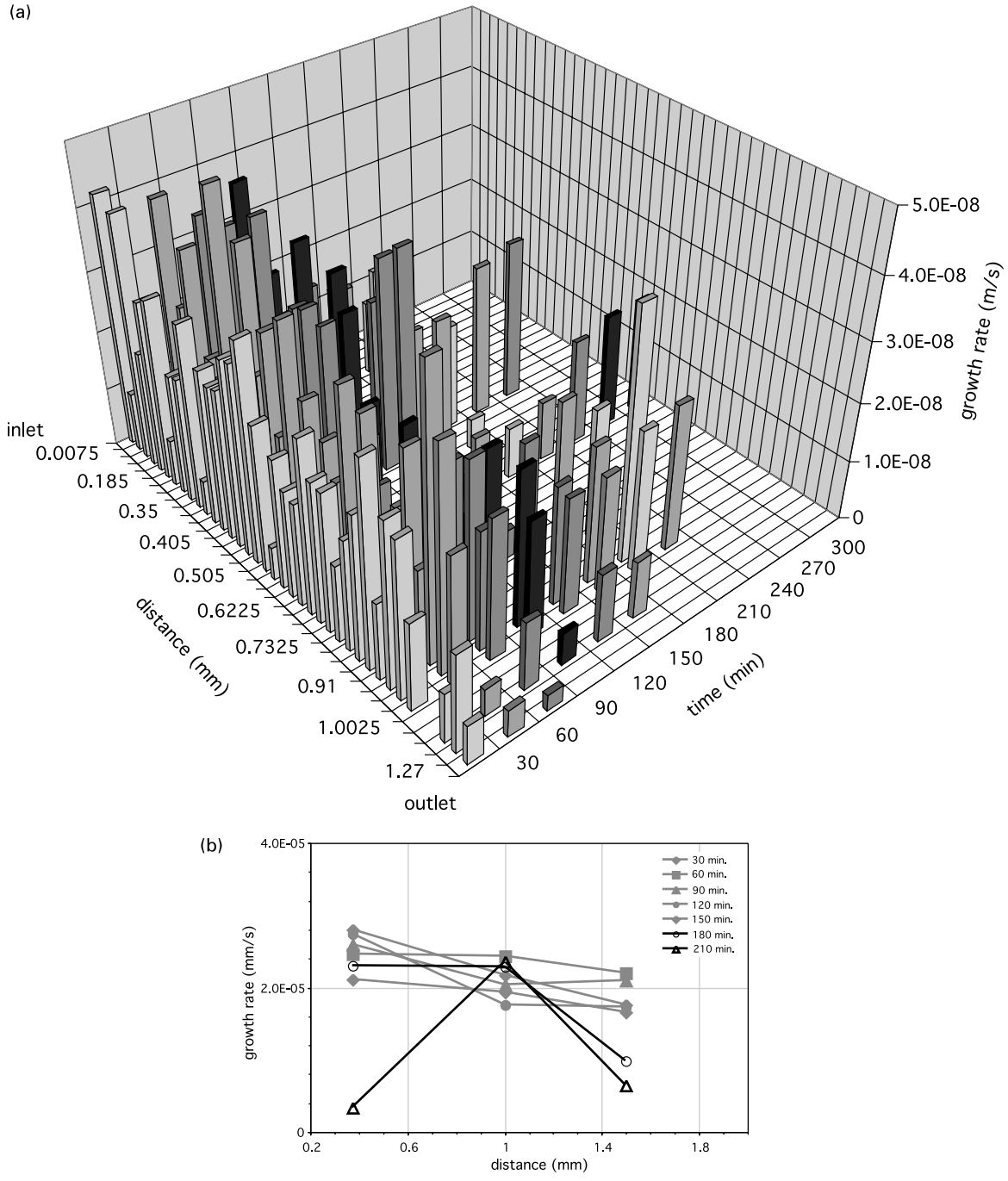

Fig. 3. (a) Growth rate of facets measured as grown distance normal to the orientation of the grain's facet. Although there is a large variation in growth rate of the individual facet over time, a decrease towards the downstream end is visible. The distance between the centre of each individual facet and the inlet was measured along a horizontal line between the inlet and outlet. Data from different time intervals are shown by different shades of grey. The uncertainty in growth rate measurement is $\pm 2.8 \times 10^{-9}$ m/s, corresponding to 2 pixels in the digital image. (b) Growth rate measured as grown area in three sub-areas along the crack (compare with sub-areas in Fig. 2b) over time, normalised by the length of the growth front. Similar to individual facet growth rates, the trend shows a decrease towards the downstream end. The growth behaviour changes after 150 min, when the growth rate in the central sub-area increases. The uncertainty of these measurements is estimated to be about $\pm 3.5 \times 10^{-7}$ mm/s, caused by uncertainties in locating the boundary in the digital images and by 3D effects.

Temperature of each of the four units is controlled to ±0.5°C. The temperature of the reaction cell is lower than that of the pump, producing a controlled supersaturation. Typical values are $\Delta T = 3$°C. This is achieved using carefully calibrated type K thermocouples, and a calibration cell with a thin built-in thermocouple. The system is closed, that is fluctuations of air humidity and evaporation do not influence the experiments.

Table 1
Experimental parameters

T3 fluid reservoir	31.0°C
T2 cell	27.9°C
T3 inlet, tube between reservoir 1 and cell	29.4°C
T4 outlet, tube between cell and reservoir 2	≈ 24.0°C (room temperature)
Relative supersaturation σ	0.14
Flow velocity	0.16 mm/s
Vein aperture y	0.5 mm
Vein length x	1.5 mm
Peclet number Pe	160
Damköhler number Da	4

The reaction cell itself consists of two glass plates ($1.5 \times 48 \times 28$ mm^3) with an inlet and an outlet tube (0.3 mm ID), connecting the system with the fluid containers. It is sealed with adhesive, leaving a space between the plates of 0.35 mm. Further details on the apparatus are given in Hilgers et al. (2000). An artificial substrate ('wall rock') consists of two parallel porous bands of granular alum, reduced in grain size by crushing crystals in saturated solution with a mortar. The vein accretion takes place by syntaxial growth on the walls of this simulated fracture.

The reaction cell is initially assembled dry, and the adhesive is cured at about 70°C. Then the cell is rapidly filled (manually) with fluid from the reservoir, taking care to avoid trapping air bubbles. This is done with the reservoir and cell already at their experimental temperature. Then the motor drive is engaged and the fluid is pumped through the cell, for periods of up to several days.

As described above, the experimental set-up allows the control of supersaturation and flow flux. The supersaturation can be calculated from the temperature difference between reservoir and cell, the flow velocity from the constant fluid flux and the dimensions of the model. During the experimental run the flow system is laminar, with a Reynolds number of about 0.07, well below the critical value of about 2300 (Giles, 1976, p. 96; Czichos, 1996, p. E-136) for tubular flow and even below the limit of turbulence in granular porous material (Ingebritsen and Sanford, 1999, p. 4). Observations of the movement of microscopic marker particles flowing with the fluid indicate the complexity of local velocity distribution in the channel.

The experiments were run in a transmitted light microscope, in plane polarised light. An image of 748×576 pixels was grabbed every 30 min with a Hitachi HV20C video camera, and stored on a computer hard disk. This image corresponds to a field of view of 1.9×1.4 mm^2 (Fig. 1).

After the experiments the image sequences were assembled into quicktime movies using Graphic Converter (www.lemkesoft.de) and analysed using routines available in Adobe Photoshop. Copies of the movies are available from the authors on request.

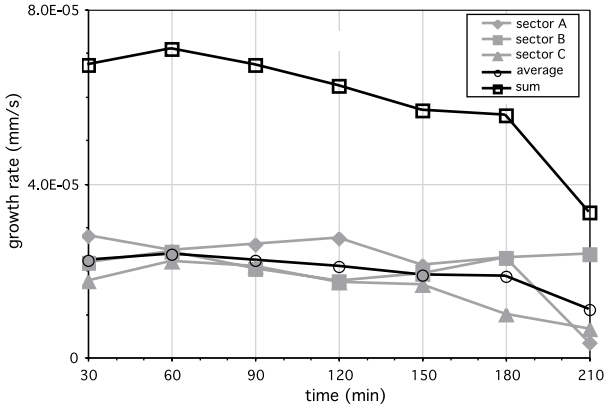

Fig. 4. Graph showing the growth rate measured from the grown area, as a function of time. Note the decrease after 150 min at which the first crystals touch each other across the channel. This decrease in growth rate is consistent with the observation of precipitation of solute on the seed crystals within the wall rock at a later stage of the experiment.

3. Experimental results

Here we present results of an experiment with relative supersaturation σ (see Appendix A for definition) of around 0.14 and fluid velocities of 0.16 mm/s, using a model material with a grain size of around 0.05 mm, where a 0.5-mm-wide opening is closed within a few hours (Table 1). The wall consists of the same material as the solute, allowing syntaxial vein growth. The values of Pe and Da for this experiment suggest that the process is dominated by advection and growth kinetics. A time series of the experiment is illustrated in Fig. 2.

The following observations can be made:

- Crystals at the upstream end grow faster than at the downstream end, resulting in the final sealing of the vein at the upstream end (Fig. 2a, number 6). Once two facing grains touch each other, the contact develops into

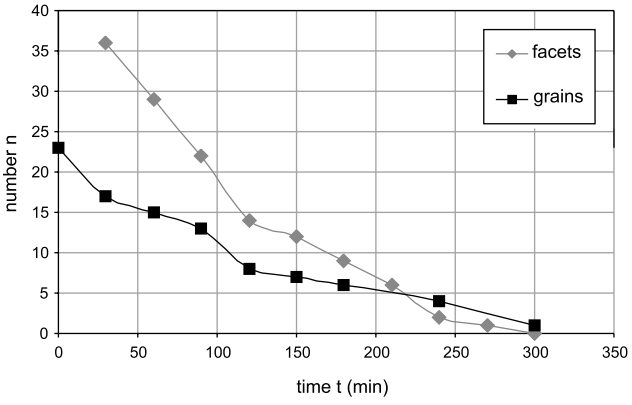

Fig. 5. Graph presenting the number of growing facets and the number of growing grains over time. This growth competition of neighbouring grains has a non-linear relationship.

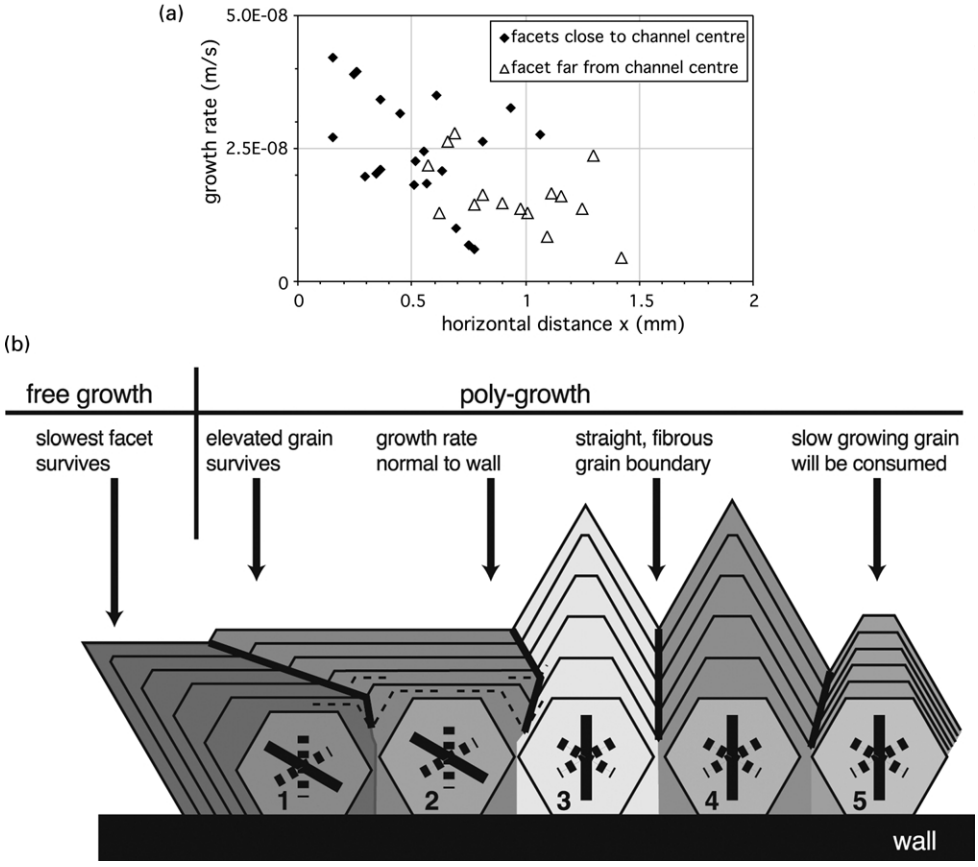

Fig. 6. (a) Plot of the average facet growth rate along the horizontal distance (x) of the vein. The seed crystals at the channel interface were subdivided in crystals near the channel centre and further away, that is in the vertical direction (y). Using the grain reaching furthest into the channel on the upper and lower interface at the initial setting, a zone of 0.21 mm width was chosen for a subdivision. Grains initially located within this zone are filled, grains further away from the channel centre are marked with open symbols. The graph suggests that grains further away from the centre (y-direction) grow slower, and indicates that the grains near the inlet grow faster than at the downstream end (x-direction). (b) Sketch illustrating the principles of growth competition in a polycrystal. Crystal facets of each individual grain move with two different velocities. Note that grains 1 to 4 have the same orthogonal growth rates. Similar to observations from single crystals, the slow growing facet of an individual grain will outgrow the faster growing facets (grain 1). An elevated grain will outgrow its neighbour, if it is in the same crystallographic orientation (grain 1/grain 2). From two neighbouring grains, the one with the faster relative facet growth rate will survive (grain 2/grain 3) Note that the orthogonal growth rates are the same for grains 2 and 3. Neighbouring grains with the same crystallographic orientation and the same elevation will develop a straight grain boundary (grain 3/grain 4). Additionally, shadowing effects are expected to cause lower growth rates during lateral fluid flow (grain 5).

a planar, optically void free grain boundary. Growth and fluid flow continue for some time after the first crystals from both sides touch, as indicated by fluid flowing into the discharge reservoir. Before flow and crystallisation stop completely, a 1-mm-long section is more or less completely filled.

- We measured the crystal growth rate by two different methods: (i) as orthogonal propagation rate of selected facets; and (ii) averaged over three sectors along the vein (here we somewhat loosely use area crystallised over time as a measure of average growth rate). It is clear from both plots (Fig. 3a and b) that the growth rate decreases along the crack, but the individual facets show a large variation in growth rate, as expected. At the point in the experiment when the two sides touch (at 150 min) there is a clear change in growth rate along the crack (Fig. 3b).
- Crystal growth activity is not restricted to the growth front at the main fluid–crystal interface. Detailed observation of the movies assembled from a series of micrographs shows that the microstructure of the porous ‘wall rock’ also undergoes changes, showing evidence for precipitation in both the pores of the wall and the channel (Fig. 4). Detailed analysis of this process was not possible due to the wall being several grains thick.
- The development of the microstructure of the vein fill is dominated by the process of growth competition. Faster growing crystals outgrow slower neighbours and produce a progressively coarser polycrystal (Fig. 2b).
- The rate of growth competition was quantified by counting the number of growing facets and grains over time, along both sides of the vein. Initially, the rate of

growth competition is high and non-linear, as shown in Fig. 5.

Similar to observations from single crystals, grains become faceted with the slowest facet surviving. However, this is not always so in our experiments where, in a number of cases, facets that first have disappeared appear again at a later stage. Polycrystal growth competition introduces additional complexity. Here, two additional processes were identified. Both are based on the principle that the grain boundary between two simultaneously growing crystals propagates in a direction determined by the orientation of the facets *and* the velocities of both facets. The first of these is the interference of two neighbouring crystals, where the growth competition between two facets growing with the same velocity is decided by their orientation with respect to the wall. Additionally, elevated grains may outgrow faster growing crystals, if their facets cover up the fast growing crystal (Fig. 6a). These effects are illustrated in Fig. 6b.

4. Numerical modelling

One of the important observations of the experiment is that growth at the upstream end of the channel is faster than at the downstream end. This can be explained by the progressive depletion of solute in the moving fluid, so that supersaturation (and the associated growth rate) decreases with distance. This process should occur in all settings where transport is from an external source, and cause the system to evolve towards self-sealing, although the length scale over which this occurs may be very different (Fig. 7). To allow comparison of our measurements with theory, we attempted to quantify this process using a simple 1D model of crystal growth from a moving fluid. In Table 1 we included the values of *Pe* and *Da* for our experiment. These indicate that advection and reaction kinetics are the important processes, and these are included in the model.

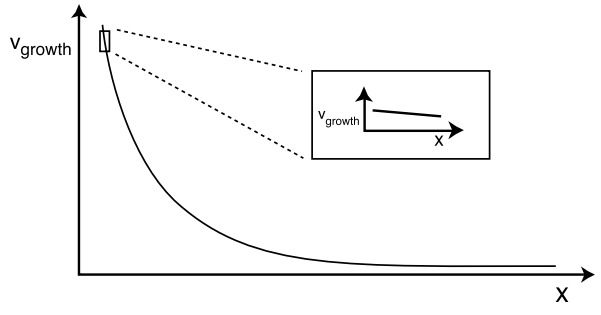

Fig. 7. Schematic diagram showing the characteristic accretion behaviour of a fracture in which solute precipitates form an advecting fluid. In such a system the growth rate always decreases along the fracture. Whether this behaviour is observed depends on the length scale available for observation (see the inset which shows a small part of this curve at a much magnified horizontal scale; in this plot the change in growth rate is not clear).

The model is similar to the one presented by Lee et al. (1996), and shows the same basic behaviour. It is based on the following assumptions, which limit its applicability to the ranges of *Da* and *Pe* relevant to our experiments:

1. Dissolved matter is transported in the *x*-direction (parallel to the flow direction) by advection alone (constant fluid flux, negligible diffusion in the *x*-direction).
2. No gradient in concentration in the fluid in the *y*-direction (perfect mixing perpendicular to the flow direction at the time scale considered).
3. No gradient in v_{flow} in the *y*-direction (plug flow).
4. No changes in temperature in the cell (either due to the heat of crystallisation or to fluid temperature being different from that of the wall).
5. Crystal growth rate v_{growth} is a function of supersaturation and v_{flow} only, and is described by a rate law which can be derived from data of crystal growth experiments in free fluid.
6. Growth is calculated in the *y*-direction only.
7. The changes in volume, viscosity and density of fluid due to precipitation of dissolved matter are negligible.
8. We neglect the anisotropy in growth rates due to facetting and grain boundaries.

The model incorporates a growth rate law, which depends non-linearly on supersaturation and fluid velocity. Parameters used for this growth rate law were determined based on published crystal growth data for alum (Garside, 1977; Mullin, 1993). In these papers, the semi-empirical equation relating growth velocity with flow velocity and supersaturation is of the form:

$$v_{\text{growth}} = A v_{\text{flow}}^{n} \sigma^{m} \tag{1}$$

with A being a constant, v_{flow} the flow velocity of the fluid, σ the relative supersaturation and the exponents n and m constants.

The equation used in our simulation was calculated by fitting this equation to published crystal growth data of alum (Garside, 1977) using a non-linear regression analysis with the least-square method (Sachs, 1997, pp. 502, 560). The data clearly show the dependence of v_{growth} on σ and v_{flow}. Data published by Mullin (1993) show a similar trend but slightly higher absolute values. To honour the observed finite growth rate in a quasi-static fluid, Eq. (1) was extended with a non-zero constant as shown below.

The resulting equation for alum from the given dataset is:

$$v_{\text{growth}} = \left(6.0\sigma^{1.5}\right)\left(6.5 + 13 v_{\text{flow}}^{0.3}\right) \times 10^{-8} \tag{2}$$

where v_{flow} and v_{growth} are both in m/s. Fig. 8 presents a

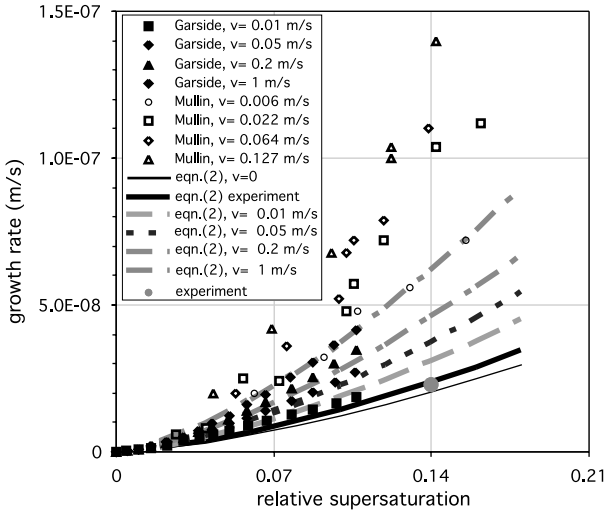

Fig. 8. Graph presenting a comparison of published data (dots) and our equation derived from the data by Garside (1977) (lines). In order to allow growth in static fluid, a dataset was introduced for $v_{flow} = 0$ following figure 5 in Garside (thin black line). Filled dots — data from Garside (1977); open dots — data from Mullin (1993); dashed lines — conditions calculated for Garside's experimental results; thin black line — conditions calculated for static fluid; thick black line — conditions calculated for the experiment; large circle — experimental set-up.

comparison of the data used and Eq. (2). Typical conditions of our experiment are indicated also.

The differential equations describing this system were numerically solved using an explicit finite difference scheme (Lasaga, 1998). Details of the calculations are given in Appendix A.

Results are in agreement with previous work on this system (Lee et al., 1996; Dijk and Berkowitz, 1998; Lasaga, 1998; Lee and Morse, 1999; Herrmann, 2000) and show that for all simulated cases there is a characteristic length X^* at which the supersaturation and the associated growth rate decreases significantly. This characteristic length is, in this paper, defined as the distance along x, where the supersaturation σ reaches 10% of the initial value. The system shows similar behaviour for all combinations of input parameters. We illustrate the sensitivity to the different parameters in the following, and compare results of simulation and experiment later.

Fig. 9a shows a rapid decrease of supersaturation and corresponding growth velocity, in this case the characteristic length X^* is reached at about 25 mm from the inlet. This trend remains stable while the vein is closed. Note that the final sealing of the vein cannot be simulated by our model. The influence of an initial wall irregularity does not introduce an instability to the system (Fig. 9b). For initially non-parallel sided veins in some cases the wall morphology allows sealing of longer sections of the vein, as shown in Fig. 9c.

Changes of the input parameters flow velocity, supersaturation and aperture all have a significant effect (Fig. 9d–f). An increase of v_{flow} results in an increase of X^*. This is because the v_{flow} dependence of v_{growth} is relatively small, and thus the dominant effect is that of a faster flowing fluid, which moves a larger distance while losing the same amount of solute. The change of relative supersaturation has a similar but stronger effect as suggested by Eq. (2). An increase in σ results in an increase of v_{growth} (Fig. 9e). Thus a lower supersaturation allows homogeneous sealing over a longer distance. For parallel-sided fractures, when the aperture is large, X^* is also large. Therefore the initial stages of precipitation are distributed over a larger distance, while a much narrower fracture cannot be sealed over a very large distance (Fig. 9f).

5. Discussion

5.1. Application to 3D

Both experiments and simulations indicate more rapid growth at the inlet of the vein. Nevertheless, veins will only be sealed at the inlet region if the scale of observation is larger than X^*. In order to test lateral advection from microstructures in a natural outcrop, the length of the exposed vein must be in the range of X^*.

Typical of all simulations is that once the growth fronts touch, flow stops. In natural veins flow does not stop when the vein is sealed in one spot, because of the more tortuous flow paths available around the sealed spots. Hints to these processes were observed during our experiments, with central grains growing although the grains at the inlet touched. The principle of decreasing supersaturation and consequent reduction in growth rate should also hold for 3D when we consider a system over a length scale that is much larger than X^* and in which the fracture system can be considered to have homogeneous transport properties over this length scale.

5.2. Application to systems in nature

As shown by the experiments of Lee et al. (1996), flow-through laboratory experiments on polycrystal growth are useful tools for the understanding of natural veins. Because laboratory experiments are necessarily done at much shorter timescales than natural systems, a discussion of the extrapolation of laboratory simulations to nature is required.

As discussed by Lee et al. (1996), for calcite under low temperature conditions the major paradox of precipitation from channelled flow lies in the unrealistically high fluid flow velocity of tens to thousands of centimetres per hour required to seal a vein over length scales of 10 cm, for geologically reasonable supersaturations. The authors point out that a low supersaturation needs very large fluid volumes to produce a given amount of precipitated material. However, it has to be kept in mind that several mechanisms have been proposed that may allow much higher supersaturations, for example clay-coating of matrix grains

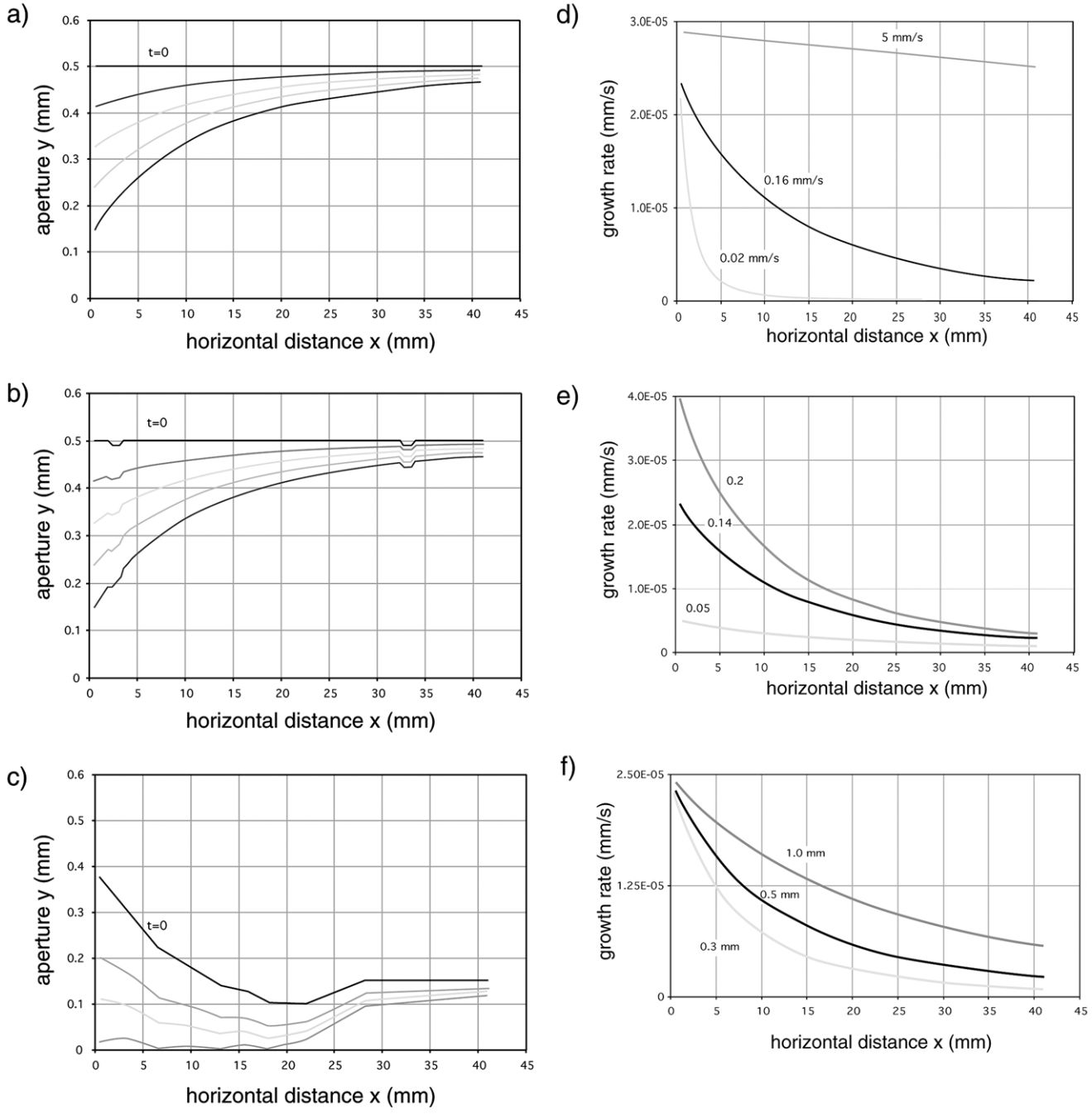

Fig. 9. (a) Numerical simulation for the conditions of the experiment (aperture = 0.5 mm, supersaturation = 0.14, v_{flow} = 0.16 mm/s). Abscissa represents the lower vein–wall interface, the black parallel line the upper vein–wall interface at time $t = 0$ s. Over time, precipitation of material takes place on the upper vein–wall interface only, causing sealing of the inlet (grey lines). Each line represents a time increment of 1 h. (b) Simulation showing that wall instabilities, introduced at $x = 3$ and 33 mm, have no positive feedback on the sealing potential of a vein. Grey lines: time increments of 1 h. (c) A wedge-shaped initial wall morphology has a potential to seal the vein homogeneously, if the aperture decreases towards the downstream end. Note that the final sealing cannot be simulated with the numerical model. Grey lines: time increments of 1 h. (d) Change of the flow velocity. An increase leads to homogeneous sealing at the scale of observation, while a decrease will seal the inlet. Black line — experimental setting (0.16 mm/s). (e) Change of the supersaturation. A decrease results in quasi-homogeneous precipitation at the scale of observation, but the rate of precipitation is low. Black line — experimental setting (0.14). (f) At constant flow velocity, an increase of the aperture will cause an increase of the rate in sealing. Black line — experimental setting (0.5 mm).

(Ortoleva et al., 1995), organic complexing (Surdam and MacGowan, 1987; Bennett et al., 1988) or silica releasing reaction from decomposition of feldspar, mica or smectite breakdown (Ross et al., 1994).

In our experiments we used a fast-growing highly soluble model material. One has therefore to ask the question of how far experiments with alum are useful as models for natural systems. Different authors use similar growth rate

laws to describe precipitation of crystals (Garside, 1977; Rimstidt and Barnes, 1980; Mullin, 1993; Lee et al., 1996; Lee and Morse, 1999). In these equations the rate of mass accumulation is proportional to the flow velocity and to the supersaturation raised to a power m, where m is an indicator of the reaction order. The growth law for alum is of the same form. Therefore, if the results are scaled with respect to the different times, supersaturations and flow rates, our results should be comparable with natural systems evolving under isothermal conditions. For the study of systems with a large temperature gradient one has to include the temperature dependence to the growth rate and supersaturation (e.g. Rimstidt and Barnes, 1980).

On the length scale of individual crystals, comparison of our results depends on the growth morphology of the model system as compared with the natural prototype. Although the general principles of growth competition and microstructural evolution discussed above should hold for most phases, direct comparison of the model with, for example, quartz would require a model material that crystallises in the same crystal system with the same dominant habit.

On the other hand, our results point the way to the need for much more complex models before we can fully understand this system. It is clear that the large local variability and anisotropic growth (Bons, 2000; Koehn et al., 2000; Hilgers et al., 2001) due to the presence of evolving crystal faces in contact with a moving fluid is not included in any of the models published so far.

5.3. The final sealing of a vein

Because open cavities are infrequent in many natural veins, one must suppose that additional processes completely seal a vein. These processes can be: (i) collapse of the fracture after a drop in fluid pressure, e.g. a discharge of fluid along a hydraulic gradient, followed by pressure solution and compaction, or (ii) a different transport mechanism such as diffusion through grain boundaries (Fisher and Brantley, 1992; Fisher, 1996; the dependence of boundary diffusion on fluid pressure was discussed by Ortoleva et al. (1995); or interfacial energy driven healing of microcracks by Lemmleyn and Kliya (1960), Smith and Evans (1984) and Brantley et al. (1990)).

5.4. Validity of assumptions

Our basic numerical modelling does not take into account various parameters, which are:

1. The evolution of microstructures: grain-scale heterogeneity in growth velocity resulting in facetting and growth competition is not modelled. For horizontal segment widths of the numerical model larger than the individual size of an experimentally grown crystal, an averaged growth rate is assumed to be a reasonable approximation. Under such conditions the natural anisotropy in facet growth rates of individual crystals will be averaged.
2. The dependence of growth rate on additional parameters: Although many of the parameters outlined in the introduction influence absolute growth rates, the relative trend will be similar to the one shown above (Fig. 3). A correlation of our numerical simulation (based on experimental work by Garside (1977) and Mullin (1993)) and our experimental results give the same absolute value of the growth rate without incorporating the factors mentioned above. This indicates that our simulation is a valid first order approximation of the experiment. Ristic et al. (1997) pointed out the decrease in growth rate of deformed crystals. This might be an important effect during the initial stages vein growth, where (in the case of syntaxial accretion) epitaxial growth on the wall rock may be strongly heterogeneous, due to different dislocation densities in the grains. Note, however, that the presence of screw dislocations can facilitate crystal growth (Sherwood and Shripathi, 1993).
3. The change of growth rate of a single crystal at constant boundary conditions over time: in general, growth competition results in the survival of slower growing facets, with all other parameters constant. Therefore in real systems growth velocity should decrease with the progress of growth competition.
4. Diffusion in the fluid in the y-direction: The model assumes a perfectly mixed fluid in the y-direction. This implies that diffusion in that direction is rapid, otherwise a concentration gradient within the fluid will develop. This in turn results in far higher distances of X^* due to fluid highly supersaturated in the centre, but at equilibrium at the outer sides. The rough interface between channel and seed crystals causes additional mixing, observed during the experiments.
   Simple calculations of 1D diffusion in a saturated solution of alum suggest that for the parameters considered in our models, i.e. fractures up to a few millimetres wide, and fluid flow rates of our experiments, diffusion is sufficiently rapid to satisfy this assumption.
5. Diffusion in the fluid in the x-direction: this process is expected to be relatively slow, due to the already existing concentration gradient along the crack caused by advective fluid flow. This will drive diffusion along the crack, but will not result in a large change in concentration profile.
6. Plug flow: in a fracture with reasonably smooth walls a parabolic flow profile is more appropriate (Dijk and Berkowitz, 1998). The complex, rough surface developed during the experiment makes the flow pattern complex, with more effective mixing in the y-direction. For this reason plug flow may be a reasonable approximation.

5.5. Comparison of experiment and model calculations

The data (Fig. 3) suggest a trend of decreasing growth velocity over the length of the experiment. The large variation in growth rate of each individual facet makes it difficult to substantiate this trend. Therefore we analysed the results, by individual facet growth rates and by averaging in several ways (cf. Fig. 3b). All analyses give comparable results, and therefore a decrease of growth rate along vein length is accepted.

Model calculations using the experimental parameters show a slightly less strong trend (Fig. 10a and b). Thus either the model is incomplete or the values of input parameters are incorrect. As mentioned above, we observed fluid flow through the porosity of the wall rock during the experiment, increasing when the facing crystals at the inlet almost touched. While discrete channelled flow was active at the beginning with material grown at the vein-opening interface, more solute precipitated inside the wall rock *and* the vein-opening interface at a later stage. This is indicated in Fig. 4, showing the amount of precipitation in the channel over time. It implies that either the fluid flux decreased when the vein was partially sealed, or material precipitated on the wall rock. This means that part of the fluid flow was through matrix porosity, and thus calculation of flow velocity from the flux overestimated the real flow velocity.

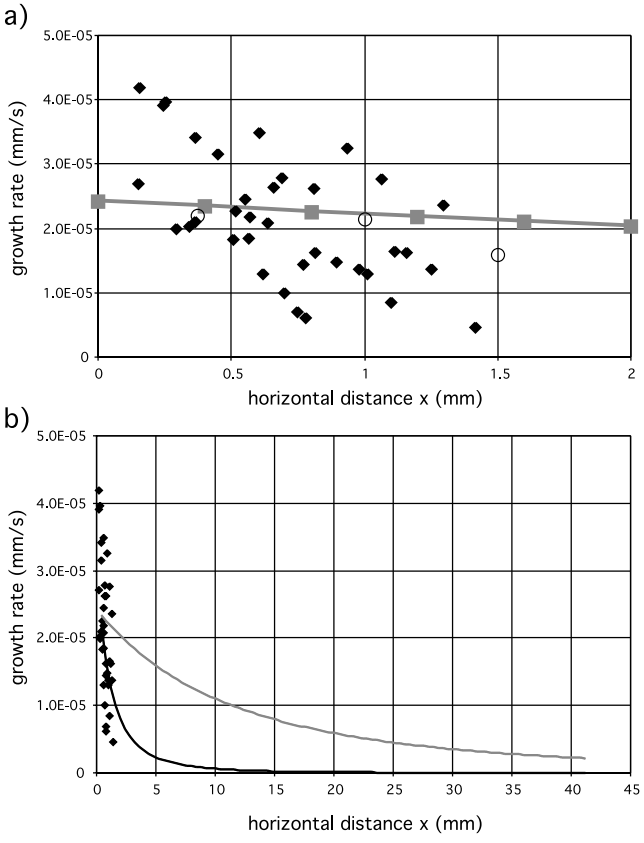

Fig. 10. (a) Comparison of experimental growth rates (dots) and numerical results (grey line). At the experimental field of view (1.5 mm), the numerical model predicts growth rates similar to those measured in the experiment from individual facets (filled dots), although the slope of the curve is too flat. Growth rates estimated from area measurements (open circles) agree well with numerical results. (b) At a larger scale (field of view 45 mm) the vein seals faster in the experiment (dots) than predicted with the model (grey line). A reduction of the flow velocity results in a steeper slope of the modelled curve (black line), comparable with experimental results (see text for discussion).

Sensitivity plots for a lower flow velocity (Fig. 9d) show that the gradient of growth rate along length increases rapidly for a decreasing flow rate. This results in a numerical trend fitting more closely with our experimental results (Fig. 10b). Therefore we propose that this is a possible explanation of the discrepancy between our measurements and simulation. Further work will involve direct measurement of the flow velocity in the experimental set-up.

The present experiments have shown that a model system is useful to study the dynamics of vein accretion at high resolution. Ongoing work is aimed at exploring the changes at longer veins, different supersaturations and flow rates. Results of these will be published in a follow-up paper.

6. Conclusions

1. Syntaxial growth experiments result in plugging of the inlet during lateral channelled flow with initially parallel walls.
2. Although the channel is blocked by a few large crystals at the inlet, further growth takes place, caused by transport through wall rock porosity.
3. In our experiment and simulations the vein remains open at the outlet, thus additional processes have to be taken into account in order to explain natural systems of completely sealed veins.
4. Grain shapes evolve due to a complicated process of growth competition, with the resulting microstructure being a result of initial crystallographic orientation and elevation of initial seed crystals.
5. Numerical simulations explain the first order trends in our experimental results, using the flow velocity and supersaturation as parameters.

Acknowledgements

Win Means, Stephen Cox and an anonymous reviewer are thanked for their suggestions, which greatly improved the manuscript. We wish to thank Werner Kraus, who invented a new technique of sealing transparent reaction cells. Discussions with Hans Herrmann and Wouter van der Zee helped to advance the numerical model. First experiments in Paul Bennema's lab introduced CH to the fundamental techniques for crystal growth in transmitted-light. JLU wishes to thank E. Juhász for the introduction to flow-through

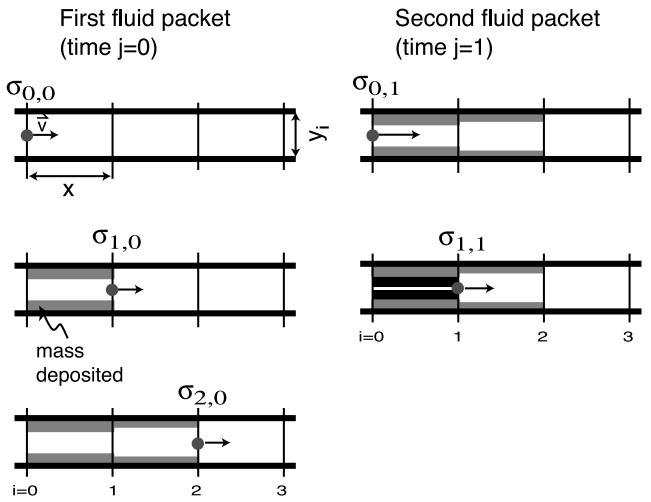

Fig. A1. Sketch of the growth process as simulated with the model. Once the first fluid pocket has flown through the tube, the following fluid volume will be inserted. The decrease in aperture causes an increase of the flow velocity. At the inlet, the relative supersaturation $\sigma_{0,j}$ equals $\sigma_{0,0}$.

crystal growth techniques. Valuable discussions with Paul Bennema, Christoph Clauser, Gernot Heger and Georg Roth are greatly acknowledged. CH was funded by Deutsche Forschungsgemeinschaft grant Ur64/1.

Appendix A. Numerical calculation scheme

For the 1D finite difference simulation, fluid packets of equal size were moved through a rectangular tube with given flow velocity and relative supersaturation (Fig. A1). The growth velocity was calculated at each node point over segment length x, with growth on the xz-plane calculated in the y-direction only.

The calculation gives a profile of supersaturation σ, flow velocity and aperture y as functions of horizontal distance x. We repeat the routine for a large number of cycles, to track the time evolution of the system (Fig. A2).

The following table shows a list of variables and values used in the finite difference calculations. Indices i and j refer to the segment number and the relative time of the process, respectively.

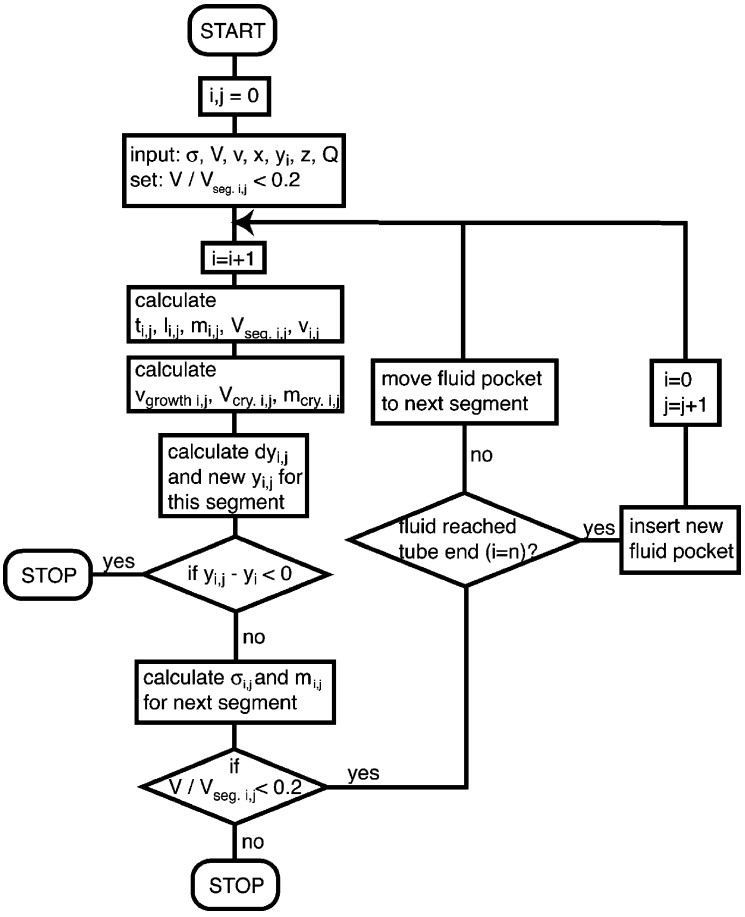

Fig. A2. Flow chart of the finite difference routine.

Table A1
List of variables and values used in the finite difference calculations. Indices *i,j* refer to the segment number and the relative time of the process, respectively

Variable	Parameter	Value
c_{eq}	Equilibrium concentration alum	(g/100 g solvent)
$c_{i,j}$	Concentration	$c_{i,j} = (\sigma_{i,j} + 1)c_{eq}$ (g/100 g solvent)
$l_{i,j}$	Fluid pocket length in x	$= V/(z \times y_{i,j})$ (mm)
$m_{i,j}$	New mass dissolved in V	$= m_{i-1,j} - m_{cry.\ i,j}$
$m_{cry.\ i,j}$	Mass crystallised	$= V_{cry.\ i,j} \times \rho$ (g/mm^3)
$m_{eq.}$	Equilibrium mass of solute	Constant (g)
Q	Initial fluid flux	$= v \times y_i \times z$ (mm^3/s)
v	Initial fluid flow velocity	0.16 mm/s
$v_{i,j}$	Local fluid flow velocity	$= Q/(y_{i,j} \times z)$ (mm/s)
$v_{growth\ i,j}$	Local growth velocity	Eq. (2) (mm/s)
V	Fluid packet volume	0.0006 mm^3
$V_{cry.\ i,j}$	Volume crystallised	$= v_{growth\ i,j} \times l_{i,j} \times z \times t_{i,j}$ (mm^3)
$V_{seg.\ i,j}$	Segment volume	$= xy_{i,j}z$ (mm^3)
$V/V_{seg.\ i,j}$	Calculation stop criterion	> 0.2
$t_{i,j}$	Time of fluid pocket in segment	$= x/v_{i,j}$ (s)
x_i	Horizontal grid size	0.4 mm
y_i	Channel aperture	0.5 mm
$y_{i,j}$	New channel aperture	$= y_{i-1,j} - dy_{i,j}$ (mm)
$dy_{i,j}$	Change in aperture	$= V_{cry.\ i,j}/(z \times x)$ (mm)
z	Channel height	0.35 mm
σ_i	Initial relative supersaturation	0.14
$\sigma_{i,j}$	Relative supersaturation	$= m_{i,j}/m_{eq.} - 1$
ρ	Density of alum	0.00172 g/mm^3

References

Bennett, P.C., Melcer, M.E., Siegel, D.I., Hassett, J.P., 1988. The dissolution of quartz in dilute aqueous solution of organic acids at 25°C. Geochimica et Cosmochimica Acta 52, 1521–1530.

Bons, P.D., 2000. The formation of veins and their microstructures. Journal of the Virtual Explorer 2, 12.

Bradley, J.S., Powley, D.E., 1994. Pressure compartments in sedimentary basins: a review. In: Ortoleva, P.J. (Ed.). Basin Compartments and Seals. AAPG Memoir 61, pp. 3–26.

Brantley, S.L., Evans, B., Hickman, H., Crerar, D.A., 1990. Healing of microcracks in quartz: implications for fluid flow. Geology 18, 136–139.

Bunsen, R., 1847. Ueber den inneren Zusammenhang der pseudovulkanischen Erscheinungen Islands. Annalen der Chemie und Pharmacie 62 (1), 1–59.

Burrus, J., 1998. Overpressure models for clastic rocks, their relation to hydrocarbon expulsion: a critical reevaluation. In: Law, B.E., Ulmishek, G.F., Slavin, V.I. (Eds.). Abnormal Pressures in Hydrocarbon Environments. AAPG Memoir 70, pp. 35–63.

Correns, C.W., 1949. Growth and dissolution of crystals under linear pressure. Discussions of the Faraday Society 5, 267–271.

Correns, C.W., Steinborn, W., 1939. Experimente zur Messung und Erklärung der sogenannten Kristallisationskraft. Zeitschrift für Kristallographie, Mineralogie und Petrographie, Abteilung A 101, 117–133.

Cox, S.F., 1999. Deformational controls on the dynamics of fluid flow in mesothermal gold systems. In: McCaffrey, K.J.W., Lonergan, L., Wilkinson, J.J. (Eds.). Fractures, Fluid Flow and Mineralization. Geological Society Special Publication 155, pp. 123–140.

Czichos, H., 1996. Hütte. Die Grundlagen der Ingenieurwissenschaften. 30th Ed.Springer, Berlin.

Deleuze, M., Brantley, S.L., 1997. Inhibition of calcite crystal growth by Mg^{2+} at 100°C and 100 bars: influence of growth regime. Geochimica et Cosmochimica Acta 61, 1475–1485.

Dijk, P., Berkowitz, B., 1998. Precipitation and dissolution of reactive solutes in fractures. Water Resources Research 34, 457–470.

Durney, D.W., Ramsay, J.G., 1973. Incremental strains measured by syntectonic crystal growth. In: de Jong, K.A., Scholten, R. (Eds.). Gravity and Tectonics, Wiley, New York. pp. 67–96.

Ellis, A.J., Mahon, W.A.J., 1977. Chemistry and Geothermal Systems. Academic Press, London.

Etheridge, M.A., Wall, V.J., Cox, S.F., Vernon, R.H., 1984. High fluid pressures during regional metamorphism and deformation: Implications for mass transport and deformation mechanisms. Journal of Geophysical Research 89, 4344–4358.

Fisher, D.M., 1996. Fabrics and veins in the forearc: a record of cyclic fluid flow at depth of <15 km. In: Bebout, G.E., Scholl, D.W., Kirby, S.H., Platt, J.P. (Eds.). Subduction: Top to Bottom. Geophysical Monograph 96, pp. 75–89.

Fisher, D.M., Brantley, S.L., 1992. Models of quartz overgrowth and vein formation: Deformation and episodic fluid flow in an ancient subduction zone. Journal of Geophysical Research 97, 20043–20061.

Garside, J., 1977. Kinetics of crystallization from solution. In: Kaldis, E., Scheel, H.J. (Eds.). Crystal Growth and Materials, North Holland, Amsterdam. pp. 484–513.

Giles, R.V., 1976. Stömungslehre und Hydraulik. McGraw Hill, Düsseldorf.

Gratier, J.P., Chen, T., Hellmann, R., 1994. Pressure solution as a mechanism for crack sealing around faults. In: U.S. Geological Survey (Ed.). The Mechanical Involvement of Fluids in Faulting. Open-file report 94-228, pp. 279–300.

Gutjahr, A., Dabringhaus, H., Lacmann, R., 1996. Studies of the growth and dissolution kinetics of the $CaCO_3$ polymorphs calcite and aragonite, II. The influence of divalent cation additives on the growth and dissolution rates. Journal of Crystal Growth 158, 310–315.

Herrmann, H., 2000. Numerische Simulation reaktiver Strömungen im porösen Untergrund am Beispiel der Lösung und Ausfällung von Quarz. Ph.D. thesis, Universität Bonn.

Hickman, S.H., Evans, B., 1995. Kinetics of pressure solution at halite–silica interfaces and intergranular clay films. Journal of Geophysical Research 100, 13113–13132.

Hilgers, C., 2000. Vein Growth in Fractures — Experimental, Numerical and Real Rock Studies. Shaker Verlag, Aachen.

Hilgers, C., Kraus, W., Urai, J.L., 2000. Development of flow-through cells for dynamic in-situ observations of crystal growth in transmitted-light microscopy. Der Präparator 46, 75–87.

Hilgers, C., Koehn, D., Bons, P.D., Urai, J.L., 2001. Development of crystal morphology during unitaxial growth in a progressively widening vein: II. Numerical simulations of the evolution of antitaxial fibrous veins. Journal of Structural Geology 23, 873–885.

Ingebritsen, S.E., Sanford, W.E., 1999. Groundwater in Geologic Processes. Cambridge University Press, Cambridge.

Kenngott, A., 1855. Mineralogische Notizen, betreffend die bekannte Species: Karstenit, Dolomit, Millerit, Turmalin, Galakit, Wasser, Plagionit, Diopsid, Zinkit, Calcit und Felsöbanit, sowie zwei neue: den Enstatit im Geschlechte der Augit-Spathe und den Pseudophit im Geschlechte der Serpentin-Steatite. Sitzungsberichte der Akademie der Wissenschaften, XVI, Mathematische Naturwissenschaftliche Classe I, 152–179.

Kharaka, Y.K., Thordsen, J.J., Evans, W.C., 1999. Geochemistry and hydromechanical interactions of fluids associated with the San Andreas fault system, California. In: Hanberg, W.C., Mozley, P.S., Moore, C.J., Goodwin, L.B. (Eds.). Faults and Subsurface Fluid Flow in the Shallow Crust. American Geophysical Union. Geophysical Monograph 113, pp. 129–148.

Koehn, D., Hilgers, C., Bons, P.D., Passchier, C.W., 2000. Numerical simulation of fibre growth in antitaxial strain fringes. Journal of Structural Geology 22, 1311–1324.

Lasaga, A.C., 1998. Kinetic Theory in the Earth Sciences. Princeton University Press, Princeton.

Lee, Y.-L., Morse, J.W., 1999. Calcite precipitation in synthetic veins: implications for the time and fluid volume necessary for vein filling. Chemical Geology 156, 151–170.

Lee, Y.-J., Morse, J.W., Wiltschko, D.V., 1996. An experimentally verified model for calcite precipitation in veins. Chemical Geology 130, 203–225.

Lemmleyn, G.G., Kliya, M.O., 1960. Distinctive features of the healing of a crack in a crystal under conditions of declining temperature. International Geology Review 2, 125–128.

Means, W.D., Li, T., 2001. A laboratory simulation of fibrous veins: some first observations. Journal of Structural Geology 23, 857–863.

Mullin, J.W., 1993. Crystallization. Butterworth-Heinemann, Oxford.

Mügge, O., 1928. Ueber die Entstehung faseriger Minerale und ihrer Aggregationsformen. Neues Jahrbuch für Mineralogie, Geologie und Paläontologie 58, 303–348.

Nicholson, K., 1993. Geothermal Fluids. Chemistry and Exploration Techniques. Springer, Berlin.

Ortoleva, P.J., 1994. Basin compartmentation: definitions and mechanisms. In: Ortoleva, P.J. (Ed.). Basin Compartments and Seals. AAPG Memoir 61, pp. 39–51.

Ortoleva, P.J., Al-Shaieb, Z., Puckette, J., 1995. Genesis and dynamics of basin compartments and seals. American Journal of Science 295, 345–427.

Putnis, A., Prieto, M., Fernandez-Diaz, L., 1995. Fluid supersaturation and crystallization in porous media. Geological Magazine 132, 1–13.

Ramsay, J.G., Huber, M., 1983. The Techniques of Modern Structural Geology. Volume 1: Strain Analysis. Academic Press, London.

Rimstidt, J.D., Barnes, H.L., 1980. The kinetics of silica–water reactions. Geochimica et Cosmochimica Acta 44, 1683–1699.

Ristic, R.I., Sherwood, J.N., Shripathi, T., 1997. The influence of tensile strain on the growth of crystals of potash alum and sodium nitrate. Journal of Crystal Growth 179, 194–204.

Ross, T.P., Rose, A.W., Poulson, S.R., 1994. Pore fluid chemistry of a pressure seal zone, Moore–Sams–Morganza gas field, Tuscaloosa Trend, Louisiana. In: Ortoleva, P.J. (Ed.). Basin Compartment and Seals. AAPG Memoir 61, pp. 139–149.

Sachs, L., 1997. Angewandte Statistik. Springer, Berlin.

Schmidegg, O., 1928. Über geregeltes Wachstumsgefüge. Jahrbuch der Geologischen Bundesanstalt 78, 1–51.

Schmidt, R., 1911. Beschaffenheit und Enstehung parallelfaseriger Aggregate von Steinsalz und Gips. PhD thesis, Universität Kiel.

Sherwood, J.N., Shripathi, T., 1993. Role of dislocations in the growth of single crystals of potash alum. Faraday Discussions 95, 173–182.

Sibson, R.H., 1990a. Faulting and fluid flow. In: Nesbitt, B.E. (Ed.). Fluids in Tectonically Active Regimes of the Continental Crust. Mineralogical Association of Canada Short Course Handbook 18, pp. 93–132.

Sibson, R.H., 1990b. Conditions for fault-valve behavior. In: Knipe, R.J., Rutter, E.H. (Eds.). Deformation Mechanisms, Rheology and Tectonics. Geological Society Special Publication 54, pp. 15–28.

Sibson, R.H., 1995. Selective fault reactivation during basin inversion: potential for fluid redistribution through fault valve action. In: Buchanan, J.G., Buchanan, P.G. (Eds.). Basin Inversion. Geological Society Special Publication 88, pp. 3–19.

Sibson, R.H., Moore, J.M., Rankin, A.H., 1975. Seismic pumping — A hydrothermal fluid transport mechansim. Journal of the Geological Society of London 131, 653–659.

Smith, D.L., Evans, B., 1984. Diffusional crack healing in quartz. Journal of Geophysical Research 89, 4125–4135.

Surdam, R.C., MacGowan, D.M., 1987. Oilfield waters and sandstone diagenesis. Applied Geochemistry 2, 127–149.

Taber, S., 1916. The origin of veins of the asbestiform minerals. Proceedings of the National Academy of Sciences 2, 659–664.

Taber, S., 1918. The origin of veinlets in the Silurian and Devonian strata of central New York. Journal of Geology 26, 56–73.

Thijssen, J.M., Knops, H.J.F., Dammers, A.J., 1992. Dynamic scaling in polycrystalline growth. Physical Review B 45, 8650–8656.

Urai, J.L., Williams, P.F., van Roermund, H.L.M., 1991. Kinematics of crystal growth in syntectonic fibrous veins. Journal of Structural Geology 13, 823–836.

Whitworth, T.M., Fritz, S.J., 1994. Electrolyte-induced solute permeability effects in compacted smectite membranes. Applied Geochemistry 9, 533–546.

Whitworth, T.M., Haneberg, W.C., Mozley, P.S., Goodwin, L.B., 1999. Solute-sieving-induced calcite precipitation on pulverized quartz sand: experimental results and implications for the membrane behavior of fault gouge. In: Hanberg, W.C., Mozley, P.S., Moore, C.J., Goodwin, L.B. (Eds.). Faults and Subsurface Fluid Flow in the Shallow Crust. Geophysical Monograph 113, pp. 149–158.

Wiltschko, D.V., Morse, J.V., 2001. Crysallization pressure versus “crack seal” as the mechanism for banded veins. Geology 29, 79–82.

Wiltschko, D., Morse, J., Sharp, Z., Lamb, W. (Eds.), 1998. Analysis of veins in low temperature environments — introduction for structural geologists, Short Course Notes for the Geological Society of America Annual Meeting, Toronto, October 24–25.

Yardley, B.W.D., 1983. Quartz veins and devolatilization during metamorphism. Journal of the Geological Society London 140, 657–663.